Trabajo de Fin de Grado:

TWO PARTICLE TRANSPORT IN TOPOLOGICAL WAVEGUIDE QED

Grado en Física
Departamento de Física de la Materia Condensada
Facultad de Ciencias

Realizado por:
Pablo Martínez Azcona

Dirigido por:
Charles Downing
Luis Martín Moreno
David Zueco

Curso 2019/20

" Rather than a Theory of Everything we appear to face a hierarchy of Theories of Things, each emerging from its parent and evolving into its children as the energy scale is lowered.[...] The central task of theoretical physics in our time is no longer to write down the ultimate equations but rather to catalogue and understand emergent behavior in its many guises, including potentially life itself. "

R. B. Laughlin and David Pines,
The Theory of Everything[1]

I would like to thank my family, without their unconditional support I would not be here today. I also want to thank my friends who have made this path much easier.

I have to thank Charles, Luis and David. They have showed me an exciting new field which I didn't know about and working with them has made me grow both as a physicist and as a person.

This work was done under a collaboration scholarship given by the MECD.

Contents

1 Introduction

1.1 An introduction to topology in physics

Topology is the branch of mathematics which studies the properties of geometric objects focusing on qualitative aspects (the number of holes or twists) rather than on metric properties (distances, volumes...). We say that two objects are equivalent if we can transform one in the other only via continuous deformations. The prototypical example of this is a mug with a handle which can be continuously deformed into a doughnut because they both have only one hole. With this, topology provides us with the tools to extend familiar concepts of real functions such as continuity and limits to functions defined in more general topological spaces. When applying topology to physics we will work with more abstract concepts than the shape of a sphere or a doughnut. The topology here refers to the quantum entanglement of wavefunctions, a system is said to be topologically trivial if it can be continuously transformed into a product state, i.e. a state in which a measurement on one of the particles does not affect the state of the other one. A phase is topological if it cannot be smoothly transformed to a trivial state.

The first discovery that paved the way to the use of topology in Condensed Matter Physics was the Integer Quantum Hall Effect (IQHE) by K. Von Klitzing [2], awarded with a Nobel prize in 1985. In the IQHE the Hall conductance of a 2D material is quantized in a series of plateaus which are related to how many Landau levels are full. The main thing that shocked Von Klitzing was that these plateaus were seen for different magnetic fields, the levels were *robust*. This means that a naive fine-tuning explanation in which the magnetic field was just right so that some Landau levels are completely filled and the rest totally empty didn't capture the physics of the system. Thouless et al. [3] proposed an explanation for this robust quantization in their TKNN formula. The connection of these results and the contemporary discovery of a geometrical phase in quantum mechanics by M.V. Berry [4] with topology was pointed out by the mathematical physicist B. Simon in [5]. Simon saw that these were related to the *first Chern class invariant of the U(1) fiber bundles*. So, each plateau in the IQHE is described by an integer which is the Chern number. This theoretical explanation, along with other remarkable contributions, was recently awarded with a Nobel Prize to D. J. Thouless, F. D. M. Haldane and J. M. Kosterlitz for "Topological phase transitions and topological phases of matter". For the full historical detail of the discoveries awarded with this Nobel prize see [6, 7].

We are used to characterize the phase transitions by local order parameters which change from one phase to the other. This is not true in topological phase transitions because the parameter that changes from one phase to the other is a topological invariant, which is not local, i.e. we need full knowledge of the bulk of the material to obtain it. The topological invariants usually have an underlying symmetry which ensures that as long that symmetry is not broken the topological invariant cannot change. This makes the topological phases very robust under perturbations, especially those that do not break the underlying symmetry.

1.2 The state of the art in topological physics

Nowadays the applications of topology in Condensed Matter Physics have extended very much. When electrons in solids have topological properties we say that we have a *topological insulator*. The fact that the material has a topologically non-trivial phase and it is surrounded by vacuum, or any other medium, which is topologically trivial, causes a localization of some states at the edges. These are called **edge states** and are recurrent in topological physics. The edge states usually have a closed band gap, this causes that insulators with a big band gap on the bulk show edge states which are conducting. The study of topological properties of bosons, mainly photons, is called *Topological Photonics*. This field covers both the interaction of photons with topological insulators and the properties of purely photonic systems, which may or may not have

an electronic counterpart. The robustness of topological phases has a lot of exciting applications, both in photonics and in nanophotonics, like the creation of a laser in the nanoscale, an overview of this field can be found in [8]. Many other experimental realizations of topological systems exist, like for example ultracold atoms, magnonic, plasmonic lattices and even quantum simulators.

One major issue in this field is the explanation of the Fractional Quantum Hall Effect(FQHE), demonstrated experimentally by D.C.Tsui et al in [9] and awarded the Nobel prize in 1998. In the IQHE the plateaus appear at integer fillings of the Landau levels, however in the FQHE there are also plateaus at fractional fillings of the Landau levels. This has led to the study of fractionally charged *anyons*, a generalization of the concept of bosons and fermions, in which the exchange of two particles adds a general phase factor $e^{i\theta}$ to the wavefunction. The FQHE is still not completely solved but interactions between the particles play a major role in its explanation. These anyons have been proposed as qubits for quantum computing because their topological nature makes them specially stable under external perturbations[10]. This points out the major importance of studying interactions in these topological systems.

1.3 Objectives

The key point we want to address in this TFG is the role of interactions in topological states. For this we will use the easiest model that exhibits topological properties, namely the Su-Schrieffer-Heeger(SSH) model, and try to see how its topological properties change when we consider particle-particle interaction. In order to be able to investigate these phenomena we will study concepts of topology in physics with some basic unidimensional topological models, numerical approaches to these models, interactions between excitations of a lattice system via a Hubbard term and quantum many body analytical techniques, like the Bethe ansatz. One interesting quasiparticle we will encounter is the doublon, a stable pair of repulsively bound bosons. However, doublons also exist for fermionic systems in which the two fermions bound with opposite spins. Aside from the fact that doublons constitute a new type of quantum light these quasiparticles are also interesting because the easiest model in which they appear, the Bose-Hubbard model, describes the transition from a Mott insulator to a superfluid. The coupling of doublons and a quasiparticle called the holon has been studied as a possible explanation for this transition [11].

This TFG is structured in the following way: In section 2 we review unidimensional tight-binding models in the second quantization formalism. Section 3 is devoted to the study of topology in the easiest topological model, the Su-Schrieffer-Heeger(SSH) model. In this section we introduce basic concepts like edge states and how to characterize their localization, topological invariants and underlying symmetries. In Section 4 we study the effect of on-site interactions between bosons on a homogeneous tight-binding model, this is called the Bose-Hubbard model. In 4.1 we study numerically the properties of this model, we find the existence of stable bound pairs of bosons even with repulsive interactions. In 4.2 we introduce an analytic technique used in quantum many body physics, the Bethe ansatz, and solve the BHM using this technique. Section 5 is devoted to the study of interactions in the SSH model with two bosonic excitations. In 5.1.1 we study numerically a limit in which results are particularly neat, the strongly dimerized limit, however, this limit has been studied more in depth by other authors. 5.1.2 is devoted to the study of a range of parameters not studied so much, the weakly dimerized limit, we numerically study the robustness of the edge states in this limit. In 5.2 we try to extend the Bethe ansatz technique to the SSH model and obtain the band structure of the system. Finally in section 6 we outline the main results obtained, propose some experimental systems suitable for the demonstration of the results and mention further lines of work in which this can be continued. All the codes used can be seen at `https://github.com/fame64/2ParticleTopologicalSSH`.

2 One-dimensional tight-binding models

The following sections 2 and 3 are devoted to the study of single particle models, i.e. we do not include particle-particle interaction. Throughout this work we set $\hbar = 1$. The general Hamiltonian in the tight-binding approximation is:

$$\mathcal{H} = \omega_0 \sum_{j=1}^{N} b_j^\dagger b_j + J \sum_{j=1}^{N} b_j^\dagger b_{j+1} + J \sum_{j=1}^{N} b_{j+1}^\dagger b_j \tag{1}$$

Where ω_0 is the on-site potential and J is the hopping constant, which is related to the probability that a particles hops to its nearest neighbour, b_j, $b_j^\dagger$ are the annihilation and creation operators in the j-th site of the chain. One should note that the combination $b_{j+1}^\dagger b_j$ first destroys one particle at site j and then creates the same particle at site $j+1$ so, the particle *hops* from j to $j+1$. As $[\mathcal{H}, \sum_j \hat{n}_j] = 0$ the Hamiltonian is number conserving, i.e. it does not create nor destroy new particles.

2.1 The dimer

We start from the most simple model, the dimer, obtained just setting $N = 2$ in (1). It describes two sites on a chain, both with the same on-site potential ω_0 and a coupling between them given by the hopping constant J. If we compute its matrix elements we find that its expression is:

$$\mathcal{H} = \begin{pmatrix} \omega_0 & J \\ J & \omega_0 \end{pmatrix} \tag{2}$$

From here it is trivial to obtain the expression of the energies and eigenstates of the system.

$$E_\pm = \omega_0 \pm J \qquad |\psi_+\rangle = \frac{1}{\sqrt{2}} \begin{pmatrix} 1 \\ 1 \end{pmatrix} \qquad |\psi_-\rangle = \frac{1}{\sqrt{2}} \begin{pmatrix} 1 \\ -1 \end{pmatrix} \tag{3}$$

Which are just symmetric and antisymmetric combinations of the states $|10\rangle$ and $|01\rangle$. $|10\rangle$ is a state representing the excitation on the first site of the chain, while the eigenstates $|\psi_\pm\rangle$ represent hybridizations of the states of the basis.

2.2 The regular chain

Now we consider the general $N > 2$ case. The Hamiltonian can be diagonalised doing a Fourier Transform.

$$b_j = \frac{1}{\sqrt{N}} \sum_k e^{ikr_j} b_k \quad b_j^\dagger = \frac{1}{\sqrt{N}} \sum_k e^{-ikr_j} b_k^\dagger \tag{4}$$

Where b_k, $b_k^\dagger$ are the creation and annihilation operators of particles with quasimomentum k. This leads to the widely known expression for the energies of a tight-binding model:

$$\omega(k) = \omega_0 - 2J \cos kl \tag{5}$$

Where k is the quasimomentum of the particle and l is the lattice constant. The Bloch Theorem tells us that the eigenfunctions of this model are of the form:

$$\phi_k(x) = e^{ikx} u_k(x) \tag{6}$$

Where $u_k(x)$ is a periodic function of x, i.e. $u_k(x + l) = u_k(x)$. In bulk systems it is common to use periodic boundary conditions (PBC). Nonetheless when dealing with topological phases

the edges will be of great interest so there is another election of boundary conditions, which we shall refer as open (or Hard) boundary conditions (OBC). PBC are typically more useful when dealing with phenomena at the bulk of the system and OBC are best describing the edge physics. We will devote most of our time to describe phenomena at the edges, for this reason we will work with OBC unless otherwise stated.

3 Topology and the Su-Schrieffer-Heeger model

The Su-Schrieffer-Heeger model (SSH) is the easiest physical system that shows topological behaviour. It was originally proposed as a description of solitons in a polyacetylene chain[12].

3.1 Tight-binding model

The SSH model is a 1D chain with a 2 atom basis. We consider two values of the hopping, the **intracell hopping** J_1 and the **intercell hopping** J_2. This opens up two possibilities, which are represented in Fig. 1 . If $J_1 > J_2$ we are in the trivial phase and the system does not show any topological behaviour at all. On the contrary, if $J_2 > J_1$ we can see in the image that the link to the edge site is weaker, this causes the existence of **edge states** which have topological nature. These edge states will be a major topic throughout this work and we will devote much of our time to understand and characterize them and the topological phases.

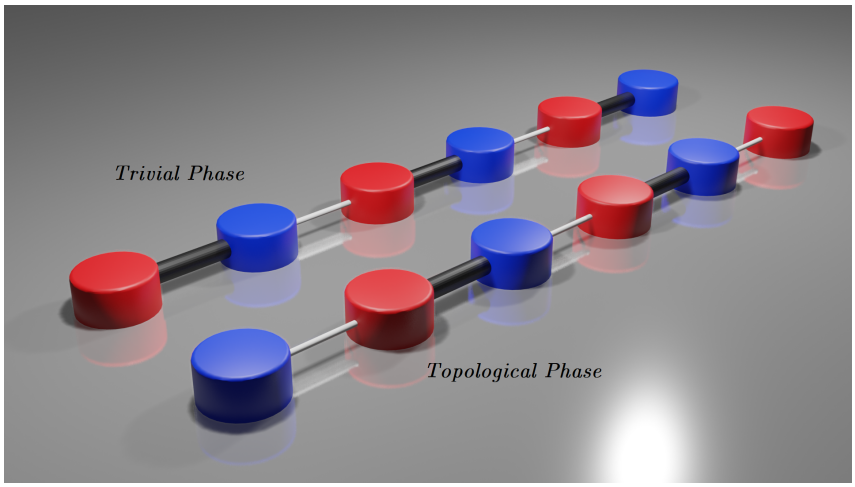

Figure 1: Artistic visualization of the SSH model. We can see the different nature in the topological and the trivial phases.

The SSH Hamiltonian is a tight-binding model with two sites per cell and two different hoppings J_1, J_2. Its Hamiltonian reads:

$$\mathcal{H} = \omega_0 \sum_{j=1}^{N/2} \sum_{\alpha=A,B} b^\dagger_{j,\alpha} b_{j,\alpha} + J_1 \sum_{j=1}^{N/2} (b^\dagger_{j,B} b_{j,A} + b^\dagger_{j,A} b_{j,B}) + J_2 \sum_{j=1}^{N/2} (b^\dagger_{j,B} b_{j+1,A} + b^\dagger_{j+1,A} b_{j,B}) \tag{7}$$

In momentum space, and assuming PBC, the Hamiltonian can be written as:

$$\hat{\mathcal{H}}(k) = \langle 0|b_k \mathcal{H} b_k^\dagger|0\rangle = \langle k|\mathcal{H}|k\rangle = \begin{pmatrix} 0 & J_1 + J_2 e^{-ik} \\ J_1 + J_2 e^{ik} & 0 \end{pmatrix} \tag{8}$$

In this expression we have taken the on-site potential as the origin to our energies $\omega_0 = 0$ and the lattice constant is taken to be 2 so that the distance between one atom and its neighbour is

1. The energies of the system can be obtained diagonalizing (8) and are given by:

$$E(k) = |J_1 + J_2 e^{-ik}| = \pm\sqrt{J_1^2 + J_2^2 + 2J_1 J_2 \cos k} \tag{9}$$

It is easy to show that the eigenstates in momentum space can be expressed as:

$$|\psi_\pm(k)\rangle = \frac{1}{\sqrt{2}} \begin{pmatrix} 1 \\ \pm e^{i\phi_k} \end{pmatrix} \qquad \phi_k = \arctan \frac{J_2 \sin k}{J_1 + J_2 \cos k} \tag{10}$$

In this TFG we will use both numerical simulations and analytical work. In the numerical side we have developed a code that computes the matrix elements directly from (7) for a finite chain and obtains the matrix eigenvalues and eigenvectors.

Fig. 2 shows the agreement between finite size simulations and the analytics. We also observe the difference between the trivial and topological phases, this difference is the energy at the boundary of the First Brillouin Zone. The topological phase presents a zero-energy state at $k = \pi$ that is not shown in the trivial phase nor predicted by the analytical expression. The reason why this state is not predicted by expression (9) is that for its obtention we have assumed periodic boundary conditions, so, we are getting rid of the edges. This zero-energy state is the so called **edge state** because it is exponentially localized at the edges, we see one example of edge state at Fig.3 (b), from Fig.3 (c) the exponential localization is clear. Those states not localized at the edges are called **bulk states**, one example of bulk state is shown in Fig.3 (a). There are many other bulk states apart from the one shown here while there is only one more edge state which looks similar to Fig.3 (b). Another interesting fact about the edge states is that they only have significant weight on one of the sublattices at each edge.

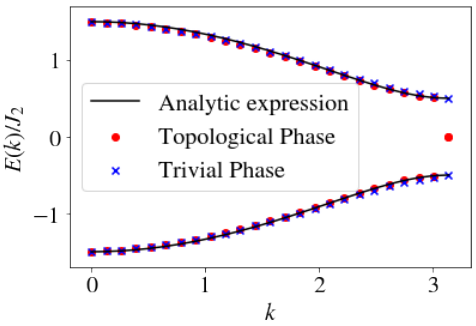

Figure 2: Dispersion relation of the SSH model in the trivial and topological phases. In the topological phase we have used $J_2 = 2J_1$, $\omega_0 = 0$ and $N = 50$. For the trivial phase $J_1 = 2J_2$.

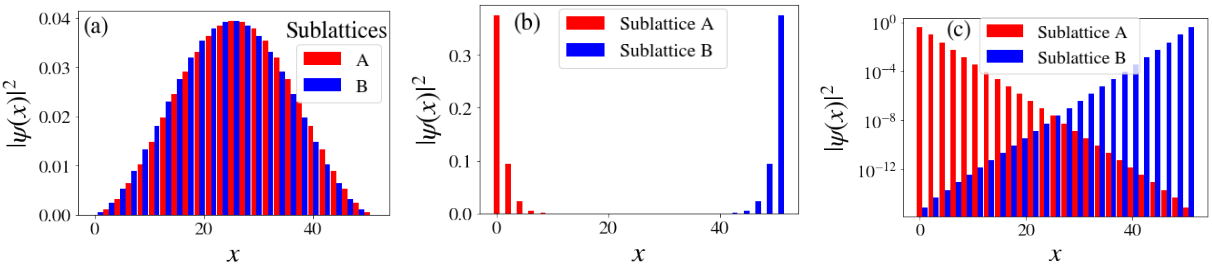

Figure 3: (a) Plot of a bulk state. (b) Plot of an edge state. (c) Plot of the same edge state in logarithmic scale. All the states have been obtained for $N = 50$, $J_2 = 2J_1$ and $\omega_0 = 0$. Red bars show $|\psi|^2$ on the sublattice A and blue ones $|\psi|^2$ on the sublattice B.

3.2 Localization and the Participation Ratio

The localization can be characterized with the **Participation Ratio** (PR). Given the normalized single particle wavefunction $|\psi\rangle = \sum_j \beta_j b_j^\dagger |0\rangle$, the PR is defined as:

$$\text{PR} := \frac{1}{\sum_j |\beta_j|^4} \tag{11}$$

A fully localized state has constant PR ~ 1 and a fully extended state has PR $\sim N$ because for a fully extended state $\beta_j = \frac{1}{\sqrt{N}}\ \forall j$ and this gives us $\sum_j \left(\frac{1}{\sqrt{N}}\right)^4 = \frac{\cancel{N}}{\cancel{N^2}} \Rightarrow \text{PR} = N$. The most relevant aspect of the Participation Ratio is its scaling with N. If PR changes proportional to N it is a bulk state. Nonetheless if we see a state whose PR stays constant with N, that state is fully localized. In our case edge states will have constant PR ~ 1.

3.3 Topological indices and the Zak phase

It is useful to write $\hat{\mathcal{H}}(k)$ in (8) as a linear combination of the Pauli matrices, $\hat{\boldsymbol{\sigma}}$ being a vector that contains the three of them. We call the vector that describes the Hamiltonian in terms of them $\mathbf{h}(k)$.

$$\hat{\mathcal{H}}(k) = \mathbf{h}(k) \cdot \hat{\boldsymbol{\sigma}} \qquad \mathbf{h}(k) = (J_1 + J_2 \cos k, J_2 \sin k, 0) \tag{12}$$

It is really interesting to plot this vector as k runs all over the first Brillouin Zone. This gives us the two plots seen in Fig. 4. In our system the $\mathbf{h}(k)$ vector is just a circumference of radius J_2 centered at $(J_1, 0)$. In the topological phase, we see that the $\mathbf{h}(k)$ plot encloses the origin, because $J_2 > J_1$ while on the trivial phase it does not. To see how this is related to topological invariants we introduce the Berry Phase.

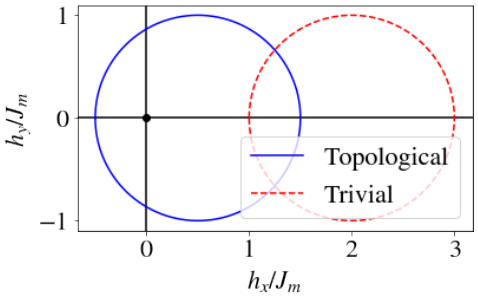

Figure 4: $\mathbf{h}(k)$ for the topological (solid blue) and trivial (dashed red) phases. For convenience in the plot we have introduced $J_m = \max(J_1, J_2)$, so that $J_m = J_2$ in the topological phase while $J_m = J_1$ in the trivial one.

3.3.1 Berry Phase

Usually in quantum mechanics we assume that the global phases of the wavefunction do not have physical meaning because we can get rid of them via a Gauge Transformation. However this is not always true. Berry[4] showed that if we have a Hamiltonian dependent on a set of parameters $\mathbf{R}(t)$ which evolves adiabatically through some curve C in parameter space, the wavefunction $|\psi(t)\rangle$ acquires a geometrical phase $e^{i\gamma_n}$ given by the expression.

$$\gamma_n(C) = i \oint_C \langle n(\mathbf{R}) | \nabla_{\mathbf{R}} n(\mathbf{R}) \rangle \, \mathrm{d}\mathbf{R} \tag{13}$$

Where $|n(\mathbf{R})\rangle$ is the eigenstate of $\mathcal{H}$ in which we start. This phase is known as the **Berry phase** and it is in fact gauge invariant. This expression can be applied to a wide range of systems, however, when applying it to a 1D solid state system like ours it is usually referred as the **Zak phase**. Zak showed in [13] that the Berry phase can be written as:

$$\phi_{Zak} = i \int_{k_i}^{k_i + G} \langle u_n | \partial_k u_n \rangle \, \mathrm{d}k \tag{14}$$

Where G is a reciprocal lattice vector. From the expression of the eigenvectors we can compute its value:

$$\partial_k |u_n\rangle = \pm \frac{1}{\sqrt{2}} \begin{pmatrix} 0 \\ \pm e^{i\phi_k} \end{pmatrix} i \frac{d\phi_k}{dk} \Rightarrow \langle u_n | \partial_k u_n \rangle = \pm \frac{i}{2} \frac{d\phi_k}{dk} \tag{15}$$

$$\phi_{Zak} = -\frac{1}{2} \int_{\mathrm{FBZ}} \frac{d\phi_k}{dk} \mathrm{d}k = -\frac{1}{2} \int_{\mathrm{FBZ}} \mathrm{d}\phi_k = -\frac{1}{2} \phi_k \Big|_{-\pi}^{\pi} = -\frac{1}{2} \arctan \frac{J_2 \sin k}{J_1 + J_2 \cos k} \Big|_{-\pi}^{\pi} \tag{16}$$

We have to be careful when evaluating this expression. If we are in the trivial phase the argument of the inverse tangent function is only on the first and fourth quadrants, so the function does not acquire any extra factor, this gives $\phi_{\text{Zak}}^{\text{Triv}} = 0$. However, if we are on the topological phase in the second quadrant the true value of the inverse tangent is $\pi - \arctan(x)$ and in the third quadrant it is $\pi + \arctan(x)$. This means that the inverse tangent has acquired an extra factor 2π. Substituting it we obtain $\phi_{\text{Zak}}^{\text{Top}} = -\pi$. This sign does not mean anything, it only appears because we have chosen the positive eigenvector in (15).

Numerical integration of (16) also gives us these values. The Berry and Zak phases are examples of **topological invariants**. No continuous deformation of the SSH system can change its Zak Phase, it is always $\phi_{Zak} = -\pi$ for the topological phase and $\phi_{Zak} = 0$ for the trivial one. This is the reason why the edge states are said to be robust, no continuous deformation of the system (like adding disorder for example) can destroy the edge states. The *winding number* counts how many times a given curve encloses the origin. In Fig. 4 we see clearly that the topological phase has $\nu = 1$ while the trivial phase has $\nu = 0$. The winding number and the Zak phase are related by $\nu = -\phi_{\text{Zak}}/\pi$. If we think about it, the $\mathbf{h}(k)$ vector or ϕ_{Zak} are quantities obtained from the bulk of the material, and it is giving us information about the edges of the system. This is a recurrent topic in topological physics and is known as the **bulk-boundary correspondence**.

3.4 Symmetries of the SSH model

We say that a Hamiltonian has **chiral symmetry** if:

$$\tilde{\Gamma}\mathcal{H}\tilde{\Gamma} = -\mathcal{H} \tag{17}$$

For our case, the chiral symmetry operator $\tilde{\Gamma}$ is σ_z. Simply multiplying the σ_z matrices with (8) we can see that the SSH model has chiral symmetry. Chiral symmetry is sometimes referred also as *sublattice symmetry* because its existence relies on the system being invariant under the interchange of sites A and B. To go from the topological phase to the trivial phase we have two options, we can either close the band gap or break chiral symmetry, none of these is a continuous transformation. If we add a term proportional to σ_z in the Hamiltonian we break chiral symmetry because (17) no longer holds. The SSH model with a term $\Delta \cdot \sigma_z$ is called the *Rice-Mele Model* and allows us to go from the topological phase to the trivial phase, this means that we may lose the edge states and it is why we say that the existence of a topological invariant like the Zak Phase relies on chiral symmetry. The edge states shown by the Rice-Mele model don't have weight on both sides of the chain because of broken chiral symmetry. Their energies are different, and the gap between them is related to Δ, the term in σ_z. It may seem that adding a constant on-site term ω_0 to the diagonal also breaks chiral symmetry because the expression (17) is not fulfilled. This is true, but as we can simply redefine our zero energy we can say that the chiral symmetry is trivially broken. However if we add a term proportional to σ_z as in the Rice-Mele model or a k dependent on-site potential $\omega(k)$ chiral symmetry is non-trivially broken. It can also be shown that SSH model has spatial *inversion symmetry* $\tilde{\Pi}\hat{\mathcal{H}}(-k)\tilde{\Pi} = \hat{\mathcal{H}}(k)$ given by $\tilde{\Pi} = \sigma_x$. Inversion symmetry is only strictly true in the bulk of the material as the existence of edges breaks it. Another symmetry of the SSH model is number conservation, because $[\mathcal{H}, \sum_j \hat{n}_j] = 0$. This means that we have a fixed number of excitations in the system.

4 Beyond the single excitation limit. The Bose Hubbard model

So far we have studied and understood the topological effects shown by the SSH model. In this section we will study another key ingredient of our work, the interaction between the particles. We consider an interaction similar to the Hubbard model. It represents an on-site interaction, and is given by the expression:

$$\mathcal{H}_{\text{int}} = \frac{U}{2}\sum_i b_i^\dagger b_i^\dagger b_i b_i = \frac{U}{2}\sum_i \hat{n}_i(\hat{n}_i - 1) \tag{18}$$

Where $b_i^\dagger,\ b_i,\ \hat{n}_i$ are, respectively, the creation, annihilation and number operators at the i-th site of the chain. U is a measure of the strength of the interaction between the particles, if $U > 0$ the interaction between the particles is repulsive and if $U < 0$ it is attractive. The tight-binding model with bosonic particles and this interaction term is known as the **Bose-Hubbard Model**. For more intricate interaction terms, such as nearest neighbour interaction, and its effect on the edge states we refer the reader to [14]. The easiest system in which to include this interaction term is a dimer. The Hamiltonian of this system is a 3×3 matrix which can be trivially diagonalized. The results are shown in Appendix 1. It is specially interesting to see the expression of the energies:

$$E_0 = \frac{U}{2} + 2\omega_0 - \sqrt{\frac{U^2}{4} + 4J^2} \qquad E_1 = 2\omega_0 + U \qquad E_2 = \frac{U}{2} + 2\omega_0 + \sqrt{\frac{U^2}{4} + 4J^2} \tag{19}$$

These expressions will be useful in the next sections. Another interesting result is that the eigenvectors in the $U \to \infty$ limit are, respectively, $|11\rangle$, $|20\rangle - |02\rangle$ and $|20\rangle + |02\rangle$. So E_0 corresponds to a symmetric combination of a boson in each site and E_1, E_2 to the antisymmetric and symmetric combination of the doubly occupied states, respectively. The Hamiltonian of the general Bose-Hubbard model is:

$$\mathcal{H} = \omega_0 \sum_{j=1}^{N} b_j^\dagger b_j - J\sum_{j=1}^{N}(b_j^\dagger b_{j+1} + b_{j+1}^\dagger b_j) + \frac{U}{2}\sum_{j=1}^{N}\hat{n}_j(\hat{n}_j - 1) \tag{20}$$

One key aspect of this Hamiltonian is that it is number conserving, because $[\mathcal{H}, \sum_j \hat{n}_j] = 0$. Thanks to the number conservation in the two excitation limit the basis can be chosen to be $\mathfrak{B} = \{|2,0,0,\ldots\rangle, |1,1,0,\ldots\rangle, |1,0,1,\ldots\rangle, \ldots, |0,2,0,\ldots\rangle, |0,1,1,\ldots\rangle, \ldots\}$. For a chain of length N it has $N(N+1)/2$ states , N of which are doubly occupied which means that they have two excitations on the same site. To see the states in this basis we have two main options. The **1D Representation** consists on summing the weight of the wavefunction in each site of the lattice, if we assume we have a $N = 3$ chain this means that the state $|0,2,0\rangle$ will have weight 2 on the second site of the lattice while the state $|1,0,1\rangle$ will have weight 1 on the first and third sites. This basis is particularly useful because $|\psi(x_i)|^2$ gives us the probability of finding a boson in the site x_i. However, there is another useful way of visualizing these states, the **2D Representation**, in it we map the 2 particle unidimensional problem into a 1 particle bidimensional problem. This means that the position on each spatial axis represents the position of each boson on the chain. Bosonic symmetry implies that $\psi(x,y) = \psi(y,x)$.

4.1 Numerical diagonalization

4.1.1 Generalization of the Participation Ratio

Now we want to obtain the fundamental properties of the Bose Hubbard Model via direct diagonalization of a finite size system. We know that we have a way of measuring how extended

is an state, the Participation Ratio. However, it was only defined for the one excitation limit, so we want to generalize that definition. If we assume that our 2 particle wavefunction is written in the form $|\psi\rangle = \lambda \sum_{m,n} \beta_{mn} b_m^\dagger b_n^\dagger |0\rangle$, where λ is some normalization factor, the PR can be defined as:

$$\mathrm{PR} := \frac{\sum_{n,m} |\beta_{nm}|^2 \lambda^2}{\sum_{n,m} |\beta_{nm}|^4 \lambda^4} \tag{21}$$

We can see that for a fully localized state it is constant and PR ~ 1 while for a fully extended state PR $\sim \frac{N(N+1)}{2}$, the number of kets on the basis. From this we see one interesting fact, the PR of a fully extended state no longer grows linearly with N but rather PR $\sim N^2$.

4.1.2 Classes of states in the Bose Hubbard Model. Doublons and Scattering States

If we obtain the finite size Hamiltonian and we diagonalize it, we see the plot in Fig. 5 (b). It is clear that adding the interaction between the particles has opened up a gap in the energy bands of our system. In Fig. 5 (b) we see have plotted the energy as a function of the index of the eigenvalue, this means that we have obtained the eigenvalues, ordered them in increasing energy and plot them. We had to do this because the definition of a wavenumber k is not trivial in the two excitation limit. We see that the energy of some states remains unchanged when we consider the interaction. This distinguishes between two classes of states in the system: The **Scattering States** that are states in which the two photons are quasi-independent, they are at different places on the lattice. This means that they only have weight on the uni-occupied states of the basis and the interaction doesn't affect their energy, it is $E_{\text{Scattering}} = E_1^{N.I.} + E_2^{N.I.}$. And the **Doublons** which are quasiparticles that represent a bound pair of two bosons, this pair is stable even for repulsive interactions. The existence and stability of the doublons has been proved experimentally [15]. In Fig. 5 (c), (d) we can see the form of a doublon in both representations. For the purpose of classifying the states the 2D representation is particularly useful as we see clearly that a given state is a doublon if it has weight on the diagonal $x = y$.

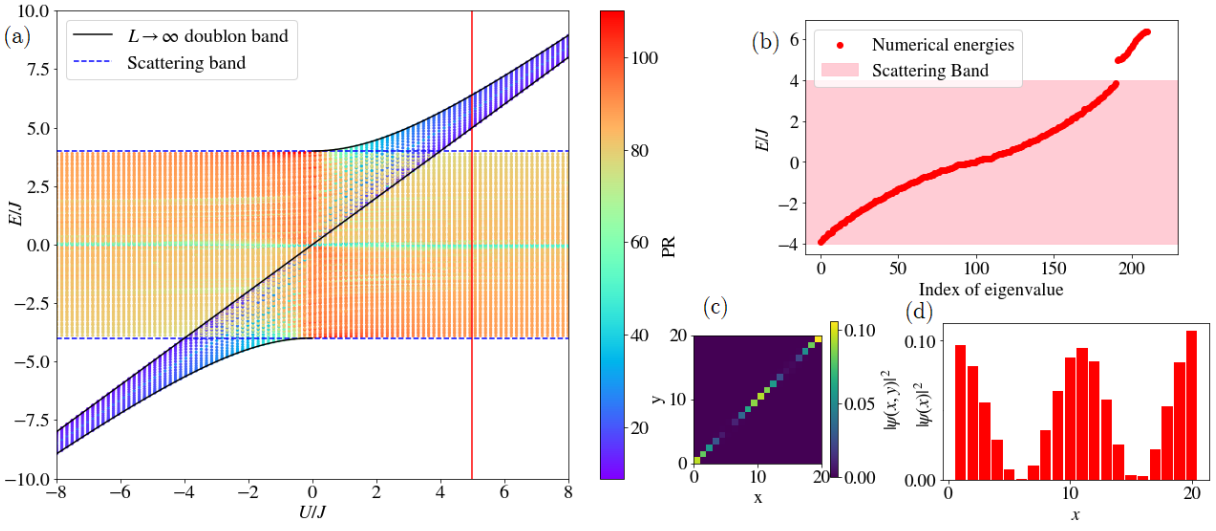

Figure 5: (a) Evolution of the system's energies as a function of U for $N = 20$ and $\omega_0 = 0$. The colorscale represents the Participation Ratio of each state. The blue and black lines correspond to the bands in the $L \to \infty$ limit in which we recover an analytical expression. The red vertical line corresponds to $U = 5J$. (b) Energies of the system for $U = 5J$. (c) A doublon 2D representation for $U = 5J$. (d) The same doublon on the 1D representation.

In Fig. 5 (a) we see the evolution of the energies as U varies. We see that when $|U|$ grows

the PR of the doublons gets smaller, in fact, in the $U \to \infty$ limit it goes to 1. This happens because we can neglect the influence of the other terms of the Hamiltonian on the doublons and as the interaction between particles is on-site, the doublons will only be localized in one site of the chain. In this same figure we also see another interesting fact, although the energy of the scattering states does not change if we change U, their wavefunction does and we see this in the PR of the scattering states, which changes a little bit with the interaction. In the $L \to \infty$ limit, there is a neat analytical expression for the doublon bands, $U \leq E \leq \sqrt{U^2 + 16J^2}$ for repulsive $U > 0$ interactions and $-\sqrt{U^2 + 16J^2} \leq E \leq U$ for attractive $U < 0$. These expressions will be discussed in section 4.2.. For repulsive interactions doublons are not energetically favourable, even though they are stable, but for attractive interactions they are the lowest energy states, i.e. they are formed spontaneously. There is a low PR state in $E = 0$ but its scaling is also PR $\sim N^2$, what means that it is still a scattering state.

As we have already pointed out, the PR of a fully extended state in the Bose-Hubbard model scales PR $\sim N^2$. However, the doublons do not obey this scaling, this happens because they are stable pairs that can be described by an effective one particle tight-binding model. So, their Participation Ratio obeys PR $\sim N$. We check this scaling in Fig. 6. We ran into an issue when we first simulated this model. There is a degeneracy that causes the PR of the doublons to stay around PR ~ 20 in $U \to \infty$ when for a fully localized state it should be PR ~ 1. To solve this problem we add a small random perturbation to the on-site potentials. We find that the optimal value is $\Delta\omega/\omega = 0.01$, so it is small but enough to break our unwanted degeneracy. In 1D systems any random perturbation to the on-site potential causes localization of the states, however, we checked that for $\Delta\omega = 1\%$ the localization length is larger than the length of the chain. This is seen in Fig. 6 where the scalings still hold.

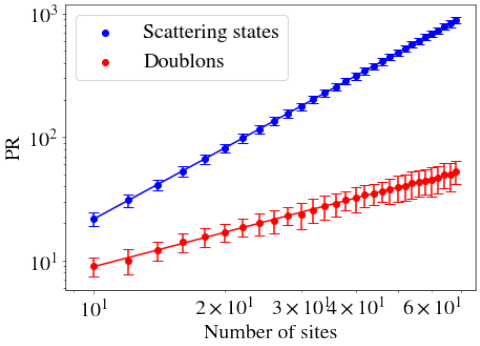

Figure 6: Scaling of the PR with N for the scattering states (blue) and the doublons(red) in log-log scale.

4.2 The Bethe ansatz

In general the Bose-Hubbard Model with N excitations is non-integrable, however, when the probability of finding three excitations on the same site vanishes, it is integrable. Concretely it is integrable via a Bethe Ansatz, this ansatz was proposed by Bethe [16] to solve analytically the 1D spin $\frac{1}{2}$ Heisenberg Model. Since then this technique has extended to many other systems, for a in-depth study of this method we refer the reader to [17]. However, we will not need such a profound knowledge and we will follow the derivations in [18, 19]. We start by assuming a wavefunction of the form $|\phi\rangle = \sum_{m,n} \phi_{mn} b_m^\dagger b_n^\dagger |0\rangle$. Substituting this wavefunction on the Hamiltonian we obtain the *recurrence relation* of the system, which reads:

$$-J(\phi_{m+1,n} + \phi_{m-1,n} + \phi_{m,n+1} + \phi_{m,n-1}) + U\delta_{mn}\phi_{mn} = E\phi_{mn} \tag{22}$$

The calculations can be seen with all detail in Appendix 2. We will work with a finite chain, for this, we take an ansatz of the form:

$$\phi_{mn} = (a_{12}e^{i(k_1 m + k_2 n)} + a_{21}e^{i(k_1 n + k_2 m)})\theta(m-n) + (a_{12}e^{i(k_1 n + k_2 m)} + a_{21}e^{i(k_1 m + k_2 n)})\theta(n-m) \tag{23}$$

Where $\theta(x)$ is the step function with $\theta(0) = 1/2$. Typically it is useful to define the centre of mass and relative variables.

$$X = \frac{m+n}{2} \quad x = m - n \quad K = k_1 + k_2 \quad k = \frac{k_1 - k_2}{2} \tag{24}$$

In these variables the expression for the Bethe Ansatz is:

$$\phi_{mn} = e^{iKX}\left(a_{12}e^{ik|x|} + a_{21}e^{-ik|x|}\right) \tag{25}$$

Substituting this ansatz in the recurrence relation for $m \neq n$ we can obtain an expression for the energies in term of K and k, the centre of mass and relative quasimomenta.

$$E = -4J\cos\frac{K}{2}\cos k = -2J(\cos k_1 + \cos k_2) \tag{26}$$

We want the expression of the energy to hold for all kinds of excitations, both doublons and scattering states. We obtain the $y(K,k)$ function, which encapsulates the relation between a_{12} and a_{21} so that (26) holds for every kind of state.

$$y(K,k) = \frac{a_{21}}{a_{12}} = -\frac{U - 4iJ\cos\frac{K}{2}\sin k}{U + 4iJ\cos\frac{K}{2}\sin k} \tag{27}$$

If we assume PBC we can obtain that the centre of mass quasimomentum is quantized, it can only take the values $K_m = \frac{2\pi m}{N}$ where $m \in \{1, 2, \ldots, N\}$. Also from PBC we can obtain the equation that the values of k have to obey.

$$(-1)^n e^{ikL} = y(K_m, k) \tag{28}$$

We can solve this equation numerically and obtain several k values for a given K_m. Substituting k in the expression for the energy we obtain the energy for that state. Doublons have imaginary k so that the state decays exponentially and it is localized. Scattering states have real k. Until now we have worked with a finite chain, this allows us to compare directly with the energies obtained numerically. However, in the infinite chain limit we can obtain some analytic expressions for both the scattering and the doublon bands, which were the ones used in Fig. 5(a) substituting $K = 0$ and $K = \pi$. This method is based on [20]. The expressions for the doublon and scattering bands are obtained in Appendix 3 and read:

$$E_{\text{Doublon}}(K) = \sqrt{U^2 + 4\left(2J\cos\frac{K}{2}\right)^2} \qquad E_{\text{Scattering}}(K) = \pm 4J\cos\frac{K}{2} \tag{29}$$

We find the solutions to (28) numerically, from there we can obtain a plot for the energies like the one shown here. From it we see that we have a continuum of states, which are the scattering states, of width $8J$. Also there is a doublon band, both of the bands fit fairly well to the analytical expressions. We check that ordering the energies obtained by the Bethe Ansatz in Fig. 7 in increasing energy we obtain a plot which matches Fig. 5 (b). In this section we have studied the properties of a topologically trivial system like the Bose Hubbard model, in the next section we will add topology to the lattice of the system. However, this is not the only way of introducing topology in these systems. One very interesting way of introducing it is shown in [21, 22]. The BHM can be extended to include a doublon hopping term, but if it is only present when hopping from site $2m$ to site $2m+1$ and not from $2m+1$ to $2m+2$, the system shows topological properties showing *interaction-induced topological states*.

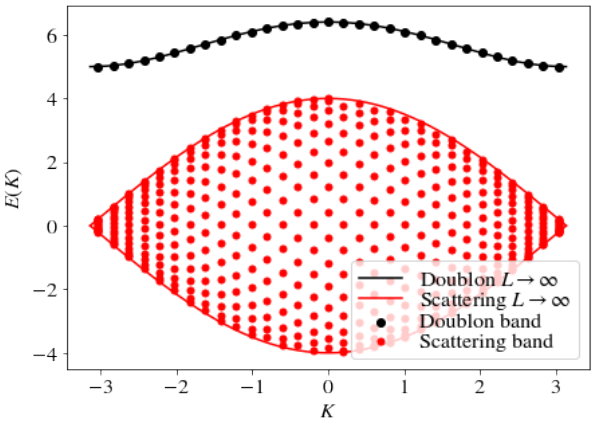

Figure 7: Dispersion relation for $N = 31$ using $\omega_0 = 0, J = 1, U = 5$.

5 Topological states in the 2 particle Su-Schrieffer-Heeger model

In this section we will study how particle-particle interaction affects the edge states. There is a limit in which most of the results are neat, this is the **Strongly dimerized limit** $J_2 \gg J_1$. However, much more work has been devoted to this limit [23, 24]. For this reason we will also study the robustness of the edge states in the **Weakly dimerized limit** where J_2 and J_1 are not so different. We don't know any references in which this limit has been studied in depth. Finally we will study analytically the two particle SSH model. All of this section is strongly based on the article by Gorlach and Poddubny [24].

5.1 Numerical diagonalization

5.1.1 Strongly dimerized limit.

Topological Phase

In Fig. 8 (a) we see the energies of the interacting SSH model in the Topological phase. The model shows 3 scattering bands whose states are analogous to the scattering states shown by the Bose-Hubbard model and two **Bulk-Edge Bands**. These states consist on one of the excitations being on the bulk while the other one is at an edge state, they already show up when we consider two excitations on the lattice without interaction, a study of this non-interacting two particle SSH model can be found at Appendix 4. There are three more bands which correspond to doublons. The energy of the three Scattering bands is $-2J_2 - 2J_1 \leq E \leq -2J_2 + 2J_1$, $-2J_1 \leq E \leq 2J_1$ and $2J_2 - 2J_1 \leq E \leq 2J_2 + 2J_1$. The energy of the Bulk-Edge bands is $-J_2 - J_1 \leq E \leq -J_2 + J_1$ and $J_2 - J_1 \leq E \leq J_2 + J_1$. These expressions can be found trivially from (9). In Fig. 8 (b) we show the PR of the states as a function of the energy. From this plot we see that the intermediate scattering band has lower PR than the other two scattering bands, we will see that this does not imply any different behaviour of these scattering bands. There is a state with very low PR, which is the **Scattering Edge State**. Besides these bands we also see three doublon bands. The two most energetic bands can be understood as the doublon band on Fig. 5 (b) but with a gap on it. We shall call the upper bands High Energy Doublons and the lowest one Low Energy Doublons. In these doublon bands we have two states with very low PR, which correspond to the **Edge Doublon** and the Quasiedge doublon. The quasiedge doublon is not truly an edge state and it occurs when the 3rd lowest PR is in the low energy doublon band. This doesn't happen always because sometimes the third lowest PR is at the high energy doublon bands.

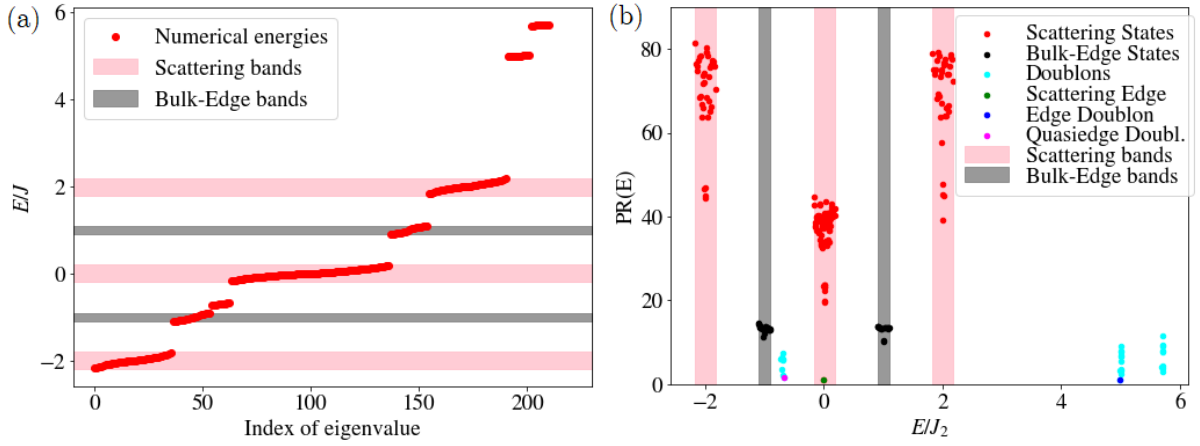

Figure 8: (a) Energy of the 2 particle SSH model for $J_1 = 0.1$ $\omega_0 = 0$ $J_2 = 1$ $U = 5$. (b) PR as a function of energy for $J_1 = 0.1$ $\omega_0 = 0$ $J_2 = 1$ $U = 5$.

In Fig. 9 we see the different classes of states shown by the system in the topological phase. Fig. 9 (a), (b) show the edge doublon, which has exponential localization, the value of the localization length ξ is the fit to an exponential function $f(x) \propto e^{x/\xi}$. It is located only at one of the edges and has weight on both sublattices. Fig. 9 (c), (d) show the scattering edge state. This state is analogous to the edge states of the one excitation SSH model. Their only difference is that in Fig. 3 (c) the sublattice A showed exponential behaviour until the other edge of the chain while now it decreases until one point and then starts growing exponentially until the edge. We are not aware of any publication in which the existence of this edge state is reported, if we work with an odd number of sites on the chain this state does not appear. Fig. 9 (e), (f) show the Quasiedge state. It is interesting because it is the third state with lowest PR however, seeing its wavefunction we see that it is not strictly at the edge. In (e) we see clearly that it has weight on the positions just right to the diagonal, this is because this state is analogous to the $|11\rangle$ eigenstate of the Bose-Hubbard dimer in $U \to \infty$. It has one particle at each position of the dimer. We will see that the strongly dimerized limit is intimately related to the eigenstates of the dimer, in fact, the low energy doublon band corresponds to $|11\rangle$ and the high energy doublon bands to the antisymmetric (intermediate energy) and symmetric (highest energy) combinations $|20\rangle \mp |02\rangle$. All the doublons at the low energy doublon band look similar to this one, all of them have weight just right to the diagonal. This means that even though the interaction term is zero because the pair is not on the same site, the dimerization forms a bound state. In (f) we see clearly that it is exponentially localized but not strictly at the edge. Fig. 9 (g) shows a Bulk-Edge state in which we see clearly that one of the excitations is at one edge and the other one is at the bulk. Fig. 9 (h) shows a bulk Doublon, we note that it is located mainly on one pair of sites, this is because one of the hoppings is very small and the bound pairs can be at whatever position on this dimer.

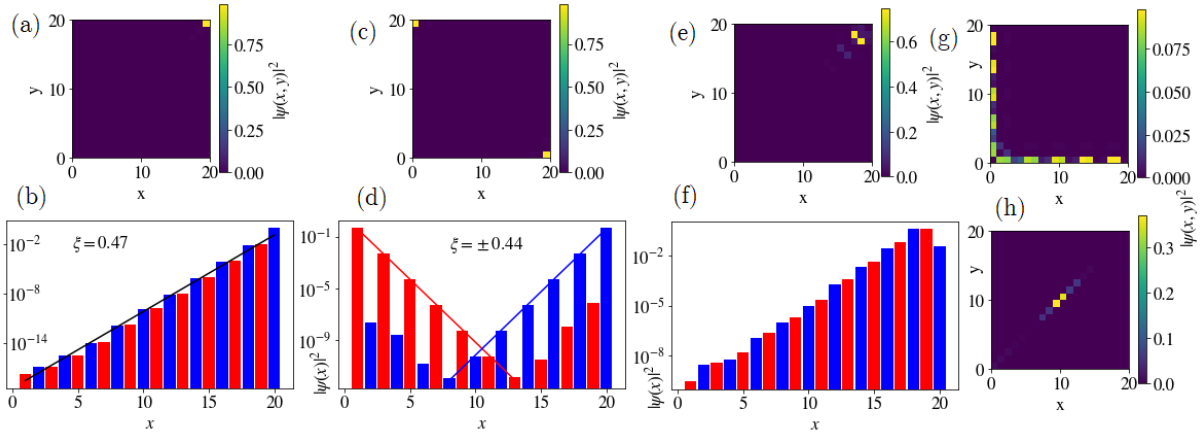

Figure 9: Classes of states at the interacting SSH model in the topological phase. (a),(b) Edge Doublon in 2D and 1D representation, note that all 1D representations are in logarithmic scale. ξ represents the localization length of the system, i.e. the fit of the wavefunction to $f(x) \propto e^{x/\xi}$. (c),(d) Scattering Edge State for the 2D and 1D representations. (e),(f) Quasiedge Doublon in the 2D and 1D representations. (g) Bulk-Edge State. (h) Bulk Doublon.

The difference between the classes of states can be seen in Fig. 10. In it we see clearly that the three scattering bands have similar scalings, PR $\sim N^2$, so the fact that the intermediate band has lower PR does not mean any significant difference in localization between the states. The bulk edge band has scaling PR $\sim N$. The three doublon bands stay with constant PR around PR ~ 2 and the three have approximately the same scaling. The minimum PR of the scattering band and the high energy doublon band, that correspond to the Scattering Edge State and the Edge Doublon stay at PR $= 1$. The Scattering Edge State has specially robust PR as it stays

strictly constant while the Edge Doublon has a little more of variation on its PR. The Quasiedge Doublon has low PR but it is bigger than that of the edge states and has bigger dispersion.

Trivial Phase

We can check the topological nature of the states described above by checking the behaviour of the system in the trivial phase. Fig. 11 (a) shows the PR of the states as a function of their energy, we see the Doublon and the Scattering bands. The fact that points out the topological nature of the Edge States described before is that we don't see a scattering state with very low PR and the minimum PR of the doublons is PR ~ 2, not like in the topological phase that was PR=1. This can be checked in Fig. 11 (b) where we plot the participation ratio of the lowest PR states as a function of N on the trivial and topological phases. In (b) we can also check that the quasiedge state does not have topological nature, as it has the same PR at both phases.

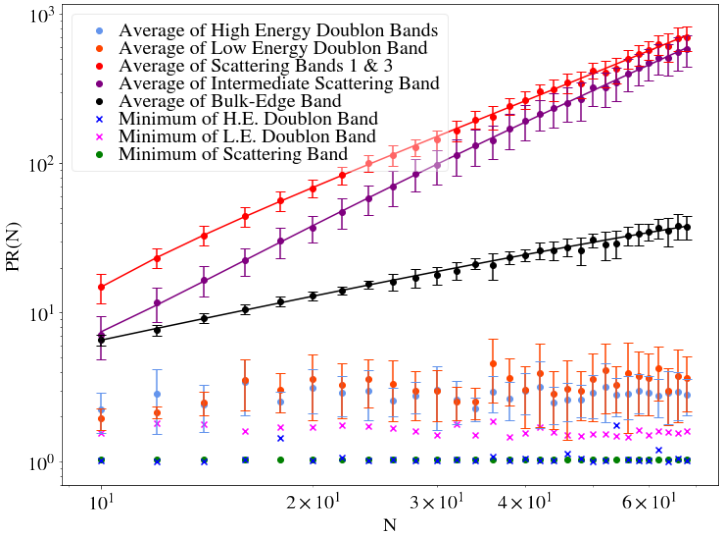

Figure 10: Evolution of PR as a function of N, the number of lattice sites, in log-log scale.

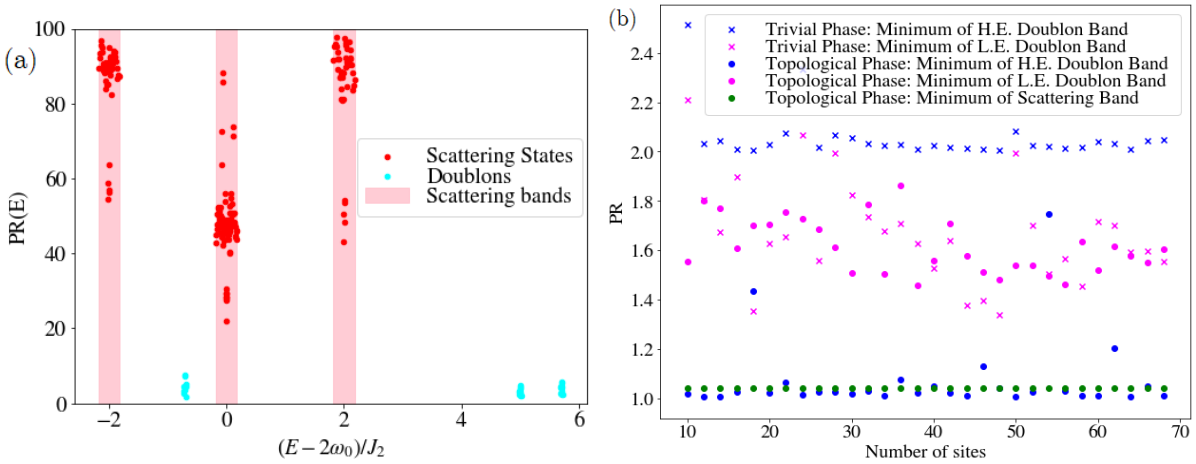

Figure 11: (a) PR as a function of E in the trivial phase, $N = 20$ $J_1 = 1$ $J_2 = 0.1$ $\omega_0 = 2$ and $U = 5$. (b) PR as a function of N for the trivial phase $J_1 = 1$ $J_2 = 0.1$ $\omega_0 = 2$ and $U = 5$.

In Fig. 12 we see different classes of states shown by the system in the trivial phase. These are not topological in nature. The state in Fig. 12 (a), (b) is the analogous state to the Edge Doublon, it is called a Tamm State, because it is an edge state which is not topological. We can see this because it has a full dimer at the edge while the edge doublon only had one site of the sublattice at the edge. Also it does not have perfect exponential localization. Fig. 12 (c), (d) show the Quasiedge Doublon in the trivial phase. It is very similar to the one in the topological phase. This fact and the scaling shown in Fig. 11 (b) proves that the quasiedge state does not have topological nature in any of the phases.

To finish our study of the interacting SSH model in the strongly dimerized limit we study the evolution of the energies, this can be seen in Fig. 13. In Fig. 13 (a) we see clearly the existence of

three scattering bands and two bulk bands whose energy is independent of U. The Doublon bands are perfectly fitted by the energies of the dimer (19) with the hopping constant $J = J_2$. This plot also shows that eigenstates $|\psi_0\rangle$ and $|\psi_2\rangle$ interchange their roles for attractive interactions $U < 0$.

This points out the intimate relation between the doublons and the eigenstates of the dimer in the strongly dimerized limit. This is reasonable because in the strongly dimerized limit a doublon is mainly localized at one of the dimers. In Fig.13 (b) we see that the antisymmetric band $|\psi_1\rangle$ is the one that has the edge doublons most of the time. This is not seen in other studies of this model like [24] where they see the doublons on the symmetric band. In this publication the authors use an odd number of sites on the lattice, but even using odd N and no perturbation on ω_0 we still see the edge states mostly on the antisymmetric band. In the article they develop a way of saying in which doublon band the edge doublons will be, using an effective 1D tight binding Hamiltonian which has a blueshift term on the on-site potential δ and an effective hopping constant t. Their conclusion is that the edge doublons are shown in the bands which obey $\delta > 2|t|$.

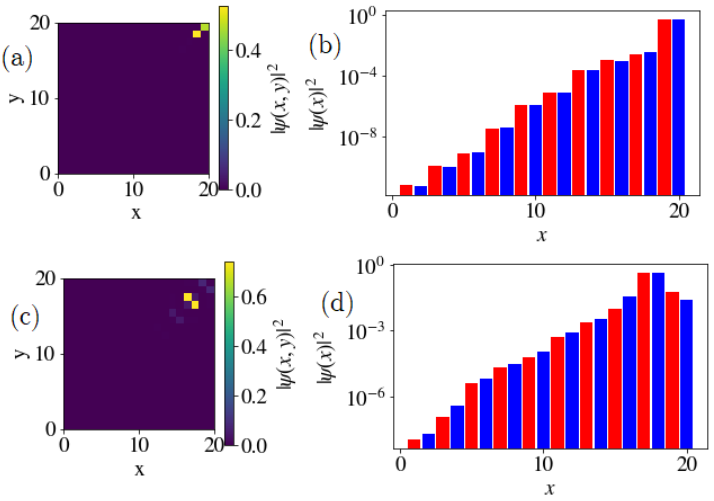

Figure 12: (a), (b) Plot of a Tamm State for the trivial phase in the 2D and 1D representations. (c), (d) Plot of the Quasiedge State for the trivial phase in the 2D and 1D representations.

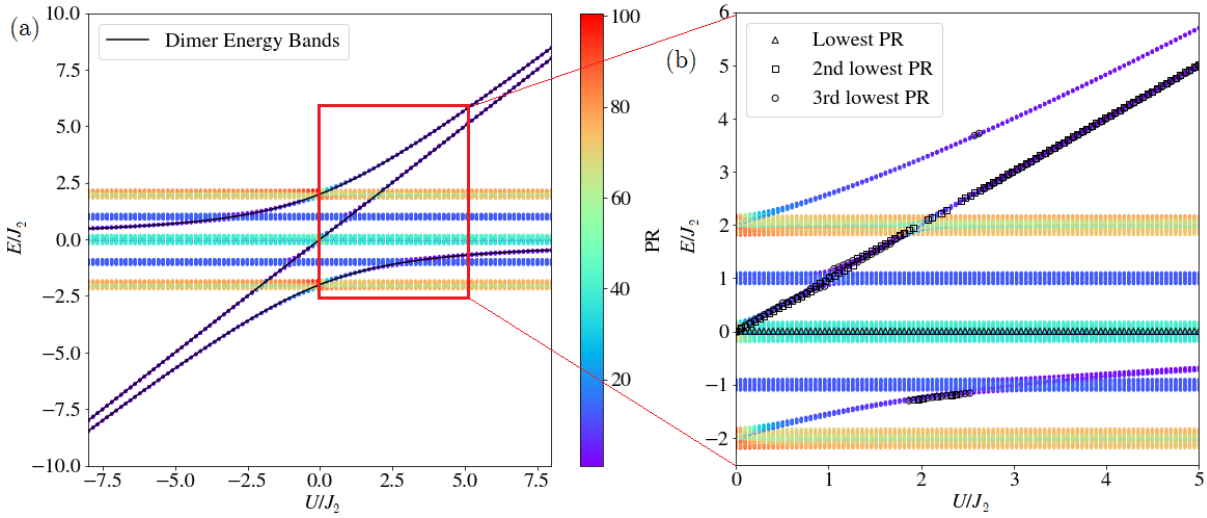

Figure 13: (a) Evolution of the energies of the system as a function of U for $N = 20$, $J_1 = 0.1J_2$, $\omega_0 = 0$. Solid lines represent the dimer energies. (b) Detail of (a), figures on top of the states represent the three lowest PR values.

Using their expressions for δ and t we obtain that the edge states should be on the symmetric upper doublon band. This is not what we see in our results, the most plausible cause for this difference is that in a chain with an even number of sites their condition for the existence of edge states changes as now there are two detuned edges, not just one. It could also be that the

expression of the parameters δ and t is different or that our doublons are on the antisymmetric band for another reason we have not taken into account.

When the third lowest PR is on the low energy band it is a quasiedge doublon, however, when it is on the high energy doublon bands it is a true edge state. This plot also shows that the scattering edge state is the one with lowest PR for all values of U, this happens with $\omega_0 = 0$ and U not super big, however, if we increase ω_0 we see that the scattering edge state starts as the lowest PR state and as $|U|$ rises it can be the second or even the third with lowest PR. Tipically the localization of the states is caused by the dimerization of the chain, however if $U \gg J_{1,2}$ and $\omega_0 \gg J_{1,2}$ we can have localization of the doublons caused by the onsite potential and the particle-particle interaction. This has been studied more in depth for the weakly dimerized limit in Appendix 5.1. Another interesting effect is that when doublon bands cross bulk or bulk-edge bands, they sometimes lose their edge states. This is known as *doublon collapse* and what happens is that doublons decay into quasi-independent particles, either scattering or bulk-edge. In fact, in [24] they show that there are four doublon bands because the antisymmetric band is split in two when it is in the scattering continuum. The doublons that stay in the continuum are unstable doublons and are only seen for values of the centre of mass quasimomentum K near the boundaries of the first Brillouin zone $|K| \sim \frac{\pi}{2}$.

5.1.2 Weakly dimerized limit

In this section we will study the robustness of the weakly dimerized limit. In this J_2 and J_1 are similar. The problem with this limit is that now the Scattering and Bulk-Edge bands overlap. This makes the distinction between the different classes of states harder than before. We can see this in Fig. 14. Also, the evolution of the doublon bands is not so clear now. This is the reason why we chose to characterize the states of the system in the strongly dimerized limit. However, we still see the edge doublons and the scattering edge state, as we see clearly in Fig. 14. The scattering edge state is the one with lowest PR, for the range of U shown here. However, for very big values of U the edge doublons and even bulk doublons can have lower PR than the Scattering Edge state. A large value of ω_0 also contributes to this. This can be seen in Appendix 5.1, where we use a very big ω_0. In the weakly dimerized limit we still see the edge doublons in the antisymmetric band.

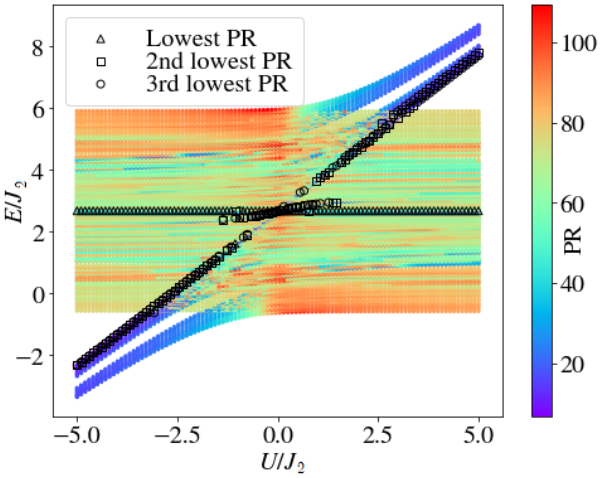

Figure 14: Evolution of the energy of the states as a function of U for the weakly dimerized limit. Parameters: $N = 20$, $\omega_0 = 2$, $J_1 = 1$, $J_2 = 1.5$

For small values of $|U|$ the second and third lowest PR correspond to a state which is not in any doublon band, but it disappears when the highest energy doublon band separates from the continuum of states. These states are interesting because they only appear on the topological phase and they can be seen in Fig. 15. They are very similar to the edge states at $U = 0$, which can be seen in Appendix 4, and these are the states which will be the edge doublons for big enough U. When there is a doublon band separated from the continuum they transform into edge doublons. We want to study their robustness against perturbations. The

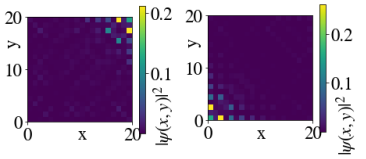

Figure 15: Edge states for $U = 0.5J_2$ in the weakly dimerized limit.

way we have decided to perturb our system is with a uniformly distributed random variation to the on-site potential $\omega_0 \to \omega_0 \in [\omega_0 - \frac{\Delta\omega}{2}, \omega_0 + \frac{\Delta\omega}{2}]$. We stress out that this is a perturbation which breaks chiral symmetry, because the two sites on the sublattice are no longer interchangeable. The system should be more robust against perturbations which maintain this symmetry. As we already pointed out in 4.1 any unidimensional system with a random perturbation on its on-site potential will have localized states. And now we won't work only with small perturbations around $\Delta\omega = 1\%$. To see the localization which comes from the topological nature and distinguish it from the localization that comes from the random perturbation to the on-site potential we will represent the difference between the minimum of PR in each phase. When $|\min(\mathrm{PR_{Top}}) - \min(\mathrm{PR_{Triv}})| \to 0$ the localization on both phases will be only caused by the random perturbation. We plot the absolute value because the topological phase has lower PR than the trivial phase.

As we don't have a clear intuition about what the results should be we first do the plots for the one excitation limit. In Fig.16 we see that, as we expected, $|\min(\mathrm{PR_{Top}}) - \min(\mathrm{PR_{Triv}})| \to 0$ as $\Delta\omega \to \omega$. If we compare (a) and (b) we see clearly that a longer chain makes the difference go faster to zero while starting at a bigger value. This is because we know that for the bulk states $\mathrm{PR} \sim N$ so the difference at $\Delta\omega = 0$ is bigger for a longer chain. The localization happens faster because each value of $\Delta\omega$ has associated a characteristic localization length. In a longer chain this localization length becomes comparable to N for a lower $\Delta\omega$.

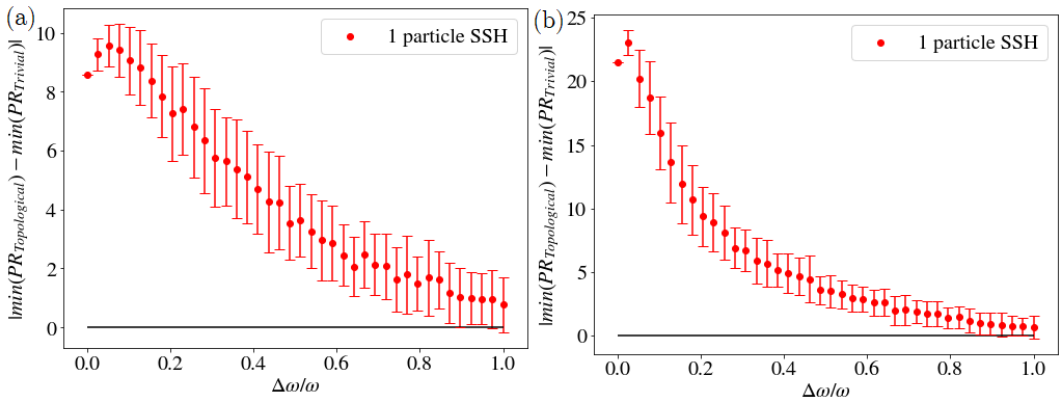

Figure 16: $|\min(\mathrm{PR_{Top}}) - \min(\mathrm{PR_{Triv}})|$ as a function of $\Delta\omega/\omega$ for the one excitation limit. The parameters are $J_2 = 1.5J_1$, $\omega_0 = 2$ for (a) $N = 20$ chain. (b)$N = 40$ chain.

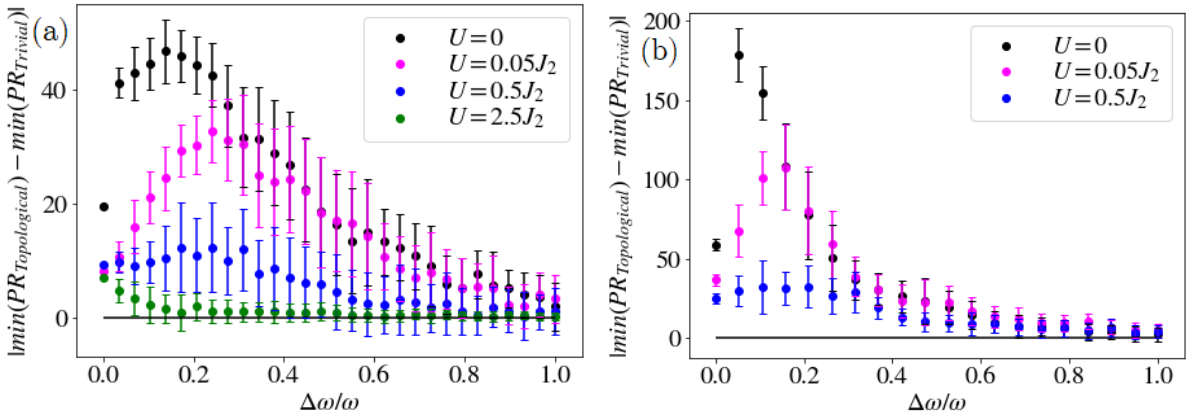

Figure 17: $|\min(\mathrm{PR_{Top}}) - \min(\mathrm{PR_{Triv}})|$ as a function of $\Delta\omega/\omega$ in the two excitation limit with parameters $J_2 = 1.5J_1$, $\omega_0 = 2$. (a) $N = 20$ chain. (b)$N = 40$ chain. U in terms of J_2 refers only to the topological phase, in the trivial phase it is the same number times J_1.

In the two excitation limit things become much more interesting because we have an extra degree of freedom to change which is U, the repulsion between the particles. We will work with repulsive interactions, however, the results are the same for U and $-U$. In Fig. 17 we see the evolution of the difference in the minimum participation ratio. As in the one excitation case the longer the chain the faster we tend to the non topological localized state. We also see that even though they have different numerical values, the shape of the $U = 0$ plot for both lengths reminds us of the shape of the 1 particle case. This is reasonable because the only difference they have is the generalization of the PR in the two excitation limit, which is bigger, but the physics of the one excitation limit and the non interacting two excitations limit should be the same. For $U < J_2$ the plots start with a positive slope. The reason for this can be seen in more detail at Appendix 5.2. Basically what is happening is that the trivial phase starts delocalizing (its PR gets bigger) for the smallest $\Delta\omega$ while the topological phase stays at constant PR, this makes the difference in localization between the two phases bigger. The other key conclusion we can get from these plots is that for a lower value of U we have more difference between the topological and trivial phases. The reason for this is that if U is big both the trivial and topological phases have very localized states, which are the doublons, so a perturbation can easily localize those doublons. However, if we have small U we have seen in Fig. 14 that the edge states are not doublons, in fact doublons do not properly exist until big enough U, this means that the most localized states in the trivial phase will have much bigger PR for small U.

After these results a natural question arises, which is the state that has the minimum of PR in the topological phase? To answer this question we will look for the position of the (x, y) coordinate with highest $|\psi(x, y)|^2$. If the maximum value of the wavefunction is at $(1, N)$ or $(N, 1)$ we will say that the state is a Scattering Edge State. If the maximum value is at $(1, 1)$ or (N, N) we will say that we have an Edge Doublon. However we have to be careful with this name because for small U the state which we are referring as edge doublon is similar to Fig. 15 which will be an Edge Doublon for bigger U but is not strictly an Edge Doublon yet. In those cases we will add an asterisk (*) to have this in mind. If the maximum is at any other place we will call that a Bulk state.

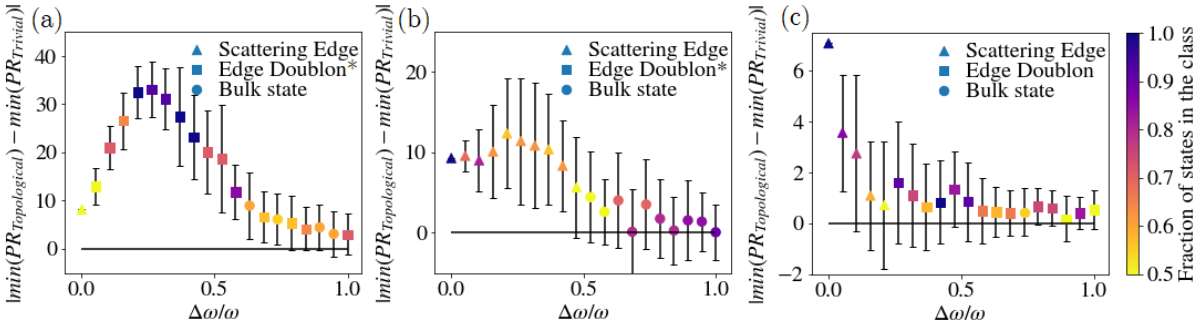

Figure 18: $|\min(\mathrm{PR_{Top}}) - \min(\mathrm{PR_{Triv}})|$ as a function of $\Delta\omega/\omega$ in the two excitation limit. The geometric shapes represent different classes of states. The colorscale represents the fraction of states in the class. A blue state represents that we are very sure that a state is in the class we say it is while a yellow state means that we are not so sure. The three plots represent different values for the interaction: (a) $U = 0.05J_2$. (b) $U = 0.5J_2$. (c) $U = 2.5J_2$.

We show the results in Fig. 18. In (a) we see that for $U = 0.05J_2$ the minimum PR is in the Edge Doublon (remember it is not strictly the Edge Doublon yet but will be for bigger U). In (b) and (c) we see that for small $\Delta\omega$ the state with lowest PR in the Topological phase is the Scattering Edge state. In the non topological localized phase we see both Edge Doublons and Bulk States. So, the Scattering Edge state found in 5.1.1 is of major importance in the weakly dimerized limit as it is the most localized excitation for every U not very close to zero. We have

also seen that the bigger U the faster trivial and topological phases have the same localization. This means that even though the energy of the Scattering Edge state is not affected by U, its robustness is, because we need a smaller $\Delta\omega$ to get the same localization in both phases.

5.2 The Bethe ansatz

In this section we apply the method of the Bethe ansatz to describe the bands of the SSH model in the two excitation limit. In [24] the authors show that the application of this technique to the two particle SSH is not so successful as it was in the BHM. The Bethe ansatz describes successfully the bulk excitations (scattering states, doublons and even bulk-edge) but breaks down when describing a finite lattice, so, we can't obtain with it the edge states. In this section we obtain analytically the scattering and bulk edge bands, the doublon band can be computed but relies on numerical solution of a system of equations and needs an extension of the ansatz, so we will not treat it. The Hamiltonian of the SSH model in the 2-excitation limit is given by:

$$\mathcal{H} = \omega_0 \sum_{j=1}^{N/2} \sum_{\alpha=A,B} b_{j,\alpha}^\dagger b_{j,\alpha} - J_1 \sum_{j=1}^{N/2} (b_{j,B}^\dagger b_{j,A} + b_{j,A}^\dagger b_{j,B}) - J_2 \sum_{j=1}^{N/2} (b_{j,B}^\dagger b_{j+1,A} + b_{j+1,A}^\dagger b_{j,B}) + \\ + \frac{U}{2} \sum_{j=1}^{N/2} \sum_{\alpha=A,B} \hat{n}_{j,\alpha}(\hat{n}_{j,\alpha} - 1) \quad (30)$$

The subindex j refers to the unit cell in which a particle is created or destroyed and the subindex $\alpha = A, B$ refers to the sublattice in which it is created or destroyed. As the system is number conserving and we only have two excitations the wavefunction of the system can be written in the form $|\psi\rangle = \sum_{\alpha,\gamma=A,B} \sum_{m,n=1}^{N/2} \beta_{mn}^{\alpha\gamma} \hat{b}_{m,\alpha}^\dagger \hat{b}_{n,\gamma}^\dagger |0\rangle$. Applying this wavefunction to the Hamiltonian and using the Schrödinger equation we obtain the recurrence relations:

$$\begin{cases} -J_1(\beta_{mn}^{BA} + \beta_{m,n}^{AB}) - J_2(\beta_{m-1,n}^{BA} + \beta_{m,n-1}^{AB}) = (\varepsilon - U\delta_{mn})\beta_{m,n}^{AA} \\ -J_1(\beta_{m,n}^{BB} + \beta_{m,n}^{AA}) - J_2(\beta_{m-1,n}^{BB} + \beta_{m,n+1}^{AA}) = \varepsilon\beta_{m,n}^{AB} \\ -J_1(\beta_{m,n}^{BB} + \beta_{m,n}^{AA}) - J_2(\beta_{m,n-1}^{BB} + \beta_{m+1,n}^{AA}) = \varepsilon\beta_{m,n}^{BA} \\ -J_1(\beta_{mn}^{BA} + \beta_{m,n}^{AB}) - J_2(\beta_{m,n+1}^{BA} + \beta_{m+1,n}^{AB}) = (\varepsilon - U\delta_{mn})\beta_{m,n}^{BB} \end{cases} \quad (31)$$

For a derivation of these equations and a derivation of the result see Appendix 6. Now we take a Bethe ansatz of the form:

$$\beta_{m,n}^{\alpha\gamma} = C^{\alpha\gamma} e^{i(k_1(m+\delta_{\alpha,B}/2)+k_2(n+\delta_{\gamma,B}/2))} \quad (32)$$

The term on $\delta_{\alpha,B}/2$ appears because we consider that the lattice parameter is 1, so, the spacing between sublattice A and B is 1/2. We also need to have in mind that even though bosonic symmetry ensures that $\beta_{mn}^{\alpha\gamma} = \beta_{nm}^{\gamma\alpha}$ in general $C^{\alpha\gamma} \neq C^{\gamma\alpha}$. From the recurrence relation we can obtain the expression of the energy in terms of the quasimomenta k_1 and k_2 of each quasi-independent boson.

$$\varepsilon = \pm\sqrt{J_1^2 + J_2^2 + 2J_1J_2\cos k_1} \pm \sqrt{J_1^2 + J_2^2 + 2J_1J_2\cos k_2} \quad (33)$$

Which is just the sum of two expressions like (9). This is because the particles in the scattering band are quasi-independent. The bulk edge band can be obtained from this but assuming that either E_{k_1} or E_{k_2} is zero. The most meaningful plots are as a function of $K = k_1 + k_2$. Plotting the bands for all the values of the relative quasimomenta q we obtain:

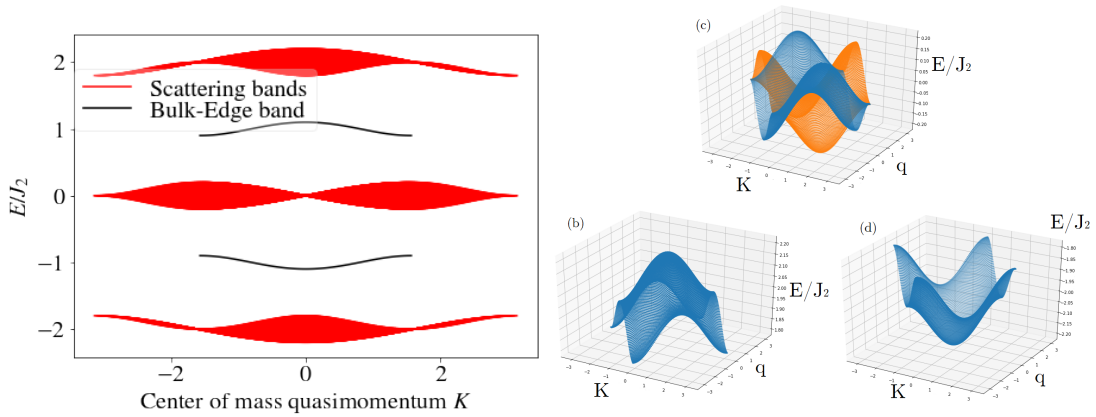

Figure 19: (a) Scattering bands plotted in blue and bulk-edge bands plotted in red. (b) 3D plot of the upper scattering band. (c) 3D plot of the intermediate scattering bands. (d) 3D plot of the lower scattering band.

In Fig. 19 we see the scattering and bulk-edge bands of the 2 particle SSH model obtained analytically. The same analysis can be carried out with the doublon bands although it does not give us nice analytical expressions for the bands and have to be solved numerically. The derivation for the doublon bands can be seen at [24]. The importance of the analytical study of this model is because it can help us obtaining a topological invariant for the 2 particle SSH model which characterizes the doublon bands and gives us information about which band hosts the edge doublons. This path is highly non trivial due to the breakdown of the Bethe ansatz, as has been discussed in [24].

6 Conclusions

6.1 Discussion of the main results

Throughout this TFG we have studied the problem of particle-particle interaction in different tight-binding models, basically the Bose-Hubbard model and the Su-Schrieffer-Heeger model. In our numerical study of the Bose-Hubbard model we found a quasiparticle called the **doublon** which is a stable bound pair of two bosons. We showed that its energy depends on U, scaling approximately $E \sim U$ for $U \to \infty$ and that the energy of the scattering states didn't depend on U. We showed also that the doublons have different localization compared to the scattering states. Then we applied an analytic technique called the Bethe ansatz to solve the BHM, and found the energy bands of the system as a function of the centre of mass quasimomentum K both for finite and infinite chains. In the $N \to \infty$ limit we found analytical expressions for the bands of the system which matched up with the results of the finite chain diagonalization and the numerical solution of the Bethe equation.

Then we studied the SSH model in the 2 excitation limit. In the strongly dimerized limit we saw a lot of different excitations. We showed that the states with topological nature were the scattering edge state, the edge doublons and the bulk-edge state. We are not aware of any publication in which they report the existence of the scattering edge state. We saw that there could be quasiedge states in the low energy doublon band which were not topological in nature and that in the trivial phase there could be Tamm states (topologically trivial edge states). Then we studied the evolution of the energy bands, checking that the evolution of the doublon bands in the strongly dimerized limit was given by the energies of the dimer and showing that the antisymmetric doublon band was the one that hosts the Edge Doublons most of the time. This has a discrepancy with other authors who see the edge states in the symmetric doublon band. After this study of the strongly dimerized limit we studied the weakly dimerized limit. In it we saw that for small $|U|$ the edge states were not edge doublons yet. We saw that the localization of the topological and trivial phases under a perturbation to the on-site potential is the same as $\Delta\omega \to \omega$. The system tends faster to equal localization of trivial and topological phases state for larger N and for bigger U. We found that the most localized state for every $|U|$ not super close to zero is the Scattering Edge state, what points out the major importance of its existence. Even though the energy of this state does not depend on U its localization does, because for bigger U it tends faster to the same localization as in the trivial phase. Finally we applied the Bethe ansatz to the SSH model, what allowed us to obtain the scattering and bulk-edge bands of the SSH model.

6.2 Experimental realization

The system we have studied during this TFG can be thought as a photonic system, because of the bosonic nature of the particles. One conceptually simple realization of these photonic systems is with coupled resonators [25]. The SSH model has been widely treated in photonics. Some of the experimental realizations include photonic superlattices, photonic crystals, electromagnetic metamaterials and plasmonic nanoparticles, further work in 1D topological photonics can be found in Sec. IV of [26]. Plasmonic nanoparticles seem to be a particularly useful platform for the study of these systems [8]. Another suitable platform for the study of this system are ultracold atoms [27]. Even though most of these systems are suited for the study of SSH model, the realization of our model, with on-site boson-boson interaction may not be easy to obtain. One way of implementing these interaction terms in systems is with quantum simulators, one potential platform are topoelectrical circuits. In [21] the authors show the formation of interaction-induced topological states. For this study they create a bidimensional circuit emulating the two particles on our lattice and have microresonators as the sites of the

2D system. However, the most promising experimental system which fully shows the 2 particle SSH physics, not being a simulation, is a superconducting quantum metamaterial like in [28]. In this article the authors study the 2 particle SSH model with a metamaterial which is an array of transmon qubits. These qubits have some properties which can be tuned to obtain the parameters of our model, the eigenfrequency of the qubits corresponds to ω_0, the coupling between the qubits represents $J_{1,2}$ and the anharmonicity of a qubit models the photon-photon interaction, which is related to U. With this metamaterial the authors study both the one and two particle SSH models. They work with an odd number of sites and attractive interactions, for this configuration they see that the edge doublon is on the symmetric band.

6.3 Future work

The main aspect which has remain opened after this work is the discrepancy between our results of which doublon band hosts the edge states. This needs further analysis, maybe the effective parameters δ and t in [24] have a different expression for an even number of sites, maybe the relation $\delta > 2|t|$ doesn't hold when there are two detuned edges or it could also be that our edge doublons in the antisymmetric band are formed for some other reason which we are not aware of. Another possible continuation of this work is to try to obtain a topological invariant which characterizes the doublon bands, in [24] the authors tried computing the Zak Phase but it did not give meaningful information, i.e. it did not say anything about which band hosted the edge doublons, for this reason they decided to use the connectivity of the vertices on a quantum walk. The breakdown of the Bethe ansatz for a finite system makes the task of finding another topological invariants specially difficult. Some other paths from this work which could unveil new exciting physics are the study of the transport properties of this model, accounting for dissipative processes which may take place, studying this same system in higher number of excitations and in other geometries or perturbing the system in new ways, for example adding a magnetic field like in [19], we think that as this perturbation does not break chiral symmetry it could show specially robust states.

References

[1] R. B. Laughlin and D. Pines. The theory of everything. *PNAS*, 97(1):28–31, 2000.

[2] K. v. Klitzing et al. New method for high-accuracy determination of the fine-structure constant based on quantized hall resistance. *Phys. Rev. Lett.*, 45:494–497, Aug 1980.

[3] D.J. Thouless et al. Quantized hall conductance in a two-dimensional periodic potential. *Phys. Rev. Lett.*, 49:405–408, Aug 1982.

[4] M.V. Berry. Quantal phase factors accompanying adiabatic changes. *P. Roy. Soc. A-Math. Phy.*, 392(1802):45–57, 1984.

[5] B. Simon. Holonomy, the quantum adiabatic theorem, and berry's phase. *Phys. Rev. Lett.*, 51:2167–2170, Dec 1983.

[6] F. D. M. Haldane. Nobel lecture: Topological quantum matter. *Rev. Mod. Phys.*, 89:040502, Oct 2017.

[7] J. M. Kosterlitz. Nobel lecture: Topological defects and phase transitions. *Rev. Mod. Phys.*, 89:040501, Oct 2017.

[8] M. S. Rider et al. A perspective on topological nanophotonics: Current status and future challenges. *J. Appl. Phys.*, 125(12):120901, 2019.

[9] D. C. Tsui et al. Two-dimensional magnetotransport in the extreme quantum limit. *Phys. Rev. Lett.*, 48:1559–1562, May 1982.

[10] V. Lahtinen and J. Pachos. A short introduction to topological quantum computation. *SciPost Phys.*, 3(3), Sep 2017.

[11] H. Yokoyama et al. Effect of doublon–holon binding on mott transition–variational monte carlo study of two-dimensional bose hubbard models. *J. Phys. Soc. Japan*, 80(8):084607, Aug 2011.

[12] W.P. Su et al. Solitons in polyacetylene. *Phys. Rev. Lett.*, 42:1698–1701, Jun 1979.

[13] J. Zak. Berry's phase for energy bands in solids. *Phys. Rev. Lett.*, 62:2747–2750, Jun 1989.

[14] M. Di Liberto et al. Two-body bound and edge states in the extended ssh bose-hubbard model. *Eur. Phys. J-Spec. Top.*, 226(12):2751–2762, Jul 2017.

[15] K. Winkler et al. Repulsively bound atom pairs in an optical lattice. *Nature*, 441(7095):853–856, Jun 2006.

[16] H. Bethe. Zur theorie der metalle. *Z. Phys.*, 71(3):205–226, Mar 1931.

[17] M. Takahashi. *Thermodynamics of One-Dimensional Solvable Models*. C. U. P., 1999.

[18] C. Boschi et al. Bound states and expansion dynamics of bosons on a one-dimensional lattice. *Phys. Rev. A*, 90, 07 2014.

[19] J. Polo et al. Exact results for persistent currents of two bosons in a ring lattice. *Phys. Rev. A*, 101:043418, Apr 2020.

[20] M. Valiente and D. Petrosyan. Two-particle states in the hubbard model. *J. Phys. B-At. Mol. Opt.*, 41(16):161002, aug 2008.

[21] N.A. Olekhno et al. Topological edge states of interacting photon pairs emulated in a topolectrical circuit. *Nat Commun 11*, 1436.

[22] A. A. Stepanenko and M. A. Gorlach. Interaction-induced topological states of photon pairs, 2020.

[23] M. Di Liberto et al. Two-body physics in the su-schrieffer-heeger model. *Phys. Rev. A*, 94:062704, Dec 2016.

[24] M. A. Gorlach and A. N. Poddubny. Topological edge states of bound photon pairs. *Phys. Rev. A*, 95:053866, May 2017.

[25] L. Lu et al. Topological photonics. *Nat. Photonics*, 8(11):821–829, Oct 2014.

[26] T. Ozawa et al. Topological photonics. *Rev. Mod. Phys.*, 91:015006, Mar 2019.

[27] N. R. Cooper et al. Topological bands for ultracold atoms. *Rev. Mod. Phys.*, 91:015005, Mar 2019.

[28] I. S. Besedin et al. Topological photon pairs in a superconducting quantum metamaterial, 2020.